Nanotechnology, Science and Applications

Dovepress

open access to scientific and medical research

Open Access Full Text Article

ORIGINAL RESEARCH

Antihistamine and Wound Healing Potential of Gold Nanoparticles Synthesized Using *Bulbine frutescens* (L.) Willd

Marizé Cuyler[1], Danielle Twilley[1], Velaphi C Thipe[2], Vusani Mandiwana[3], Michel L Kalombo[3], Suprakas S Ray[4], Rirhandzu Shamaine Rikhotso-Mbungela[4], Arno Janse van Vuuren[5], Will Coetsee[6], Kattesh V Katti[2,*], Namrita Lall[1,7–9,*]

[1]Department of Plant and Soil Sciences, University of Pretoria, Pretoria, Gauteng, 0002, South Africa; [2]Department of Radiology, Institute of Green Nanotechnology, University of Missouri, Columbia, MO, 65212, USA; [3]Chemical Cluster Centre for Nanostructures and Advanced Materials, Council for Scientific and Industrial Research, Pretoria, 0001, South Africa; [4]DST/CSIR National Centre for Nanostructured Materials, Council for Scientific and Industrial Research, Pretoria, 0001, South Africa; [5]Centre for High Transmission Electron Microscopy, Nelson Mandela University, Port Elizabeth, 6031, South Africa; [6]Botanica Natural Products Pty (Ltd), Canterbury Farm MR 254, Alldays, Limpopo, 0909, South Africa; [7]School of Natural Resources, University of Missouri, Columbia, MO, 65211, USA; [8]College of Pharmacy, JSS Academy of Higher Education and Research, Mysuru, Karnataka, 570015, India; [9]Bio-Tech Research and Development Institute, University of the West Indies 770, Kingston, Jamaica

*These authors contributed equally to this work

Correspondence: Kattesh V Katti, Department of Radiology, Institute of Green Nanotechnology, University of Missouri, Columbia, MO 65212, USA, Tel +1 (573) 882-5656, Fax +1 (573) 884-5679, Email kattik@health.missouri.edu; Namrita Lall, Department of Plant and Soil Sciences, University of Pretoria, Pretoria, Gauteng, South Africa, Tel/Fax +27 (012) 420 2524, Email namrita.lall@up.ac.za

Background: Atopic dermatitis (eczema) is an inflammatory skin condition with synthetic treatments that induce adverse effects and are ineffective. One of the proposed causes for the development of the condition is the outside-in hypothesis, which states that eczema is caused by a disruption in the skin barrier. These disruptions include developing dry cracked skin, which promotes the production of histamine. *Bulbine frutescens* (BF) is traditionally used to treat wounds and eczema; however, limited research has been conducted to scientifically validate this. Furthermore, gold nanoparticles (AuNPs) have been used to repair damaged skin; however, no research has been conducted on AuNPs synthesized using BF.

Purpose: The study aimed to determine whether BF alleviated skin damage through wound healing, reducing the production of histamine and investigate whether AuNPs synthesized using BF would enhance biological activity.

Methods: Four extracts and four synthesized AuNPs were prepared using BF and their antiproliferative and wound healing properties against human keratinocyte cells (HaCaT) were evaluated. Thereafter, the selected samples antiproliferative activity and antihistamine activity against phorbol 12-myristate 13-acetate (PMA) stimulated granulocytes were evaluated.

Results: Of the eight samples, the freeze-dried leaf juice (BFE; $p < 0.01$) extract and its AuNPs (BFEAuNPs; $p < 0.05$) displayed significant wound closure at 100 µg/mL and were further evaluated. The selected samples displayed a fifty percent inhibitory concentration (IC_{50}) of >200 µg/mL against PMA stimulated granulocytes. Compared to the untreated (media with PMA) control (0.30 ± 0.02 ng/mL), BFEAuNPs significantly inhibited histamine production at a concentration of 100 ($p < 0.01$) and 50 µg/mL ($p < 0.001$).

Conclusion: BFE and BFEAuNPs stimulated wound closure, while BFEAuNPs significantly inhibited histamine production. Further investigation into BFEAuNPs in vivo wound healing activity and whether it can target histamine-associated receptors on mast cells as a potential mechanism of action should be considered.

Keywords: atopic dermatitis, histamine production, outside-in hypothesis, scratch assay

Introduction

Eczema, also known as atopic dermatitis, is an inflammatory skin condition which is prevalent in developed countries. A proposed cause of the condition is the outside-in hypothesis, which states that eczema could occur due to a disruption

Received: 31 October 2023
Accepted: 22 February 2024
Published: 13 March 2024

Graphical Abstract

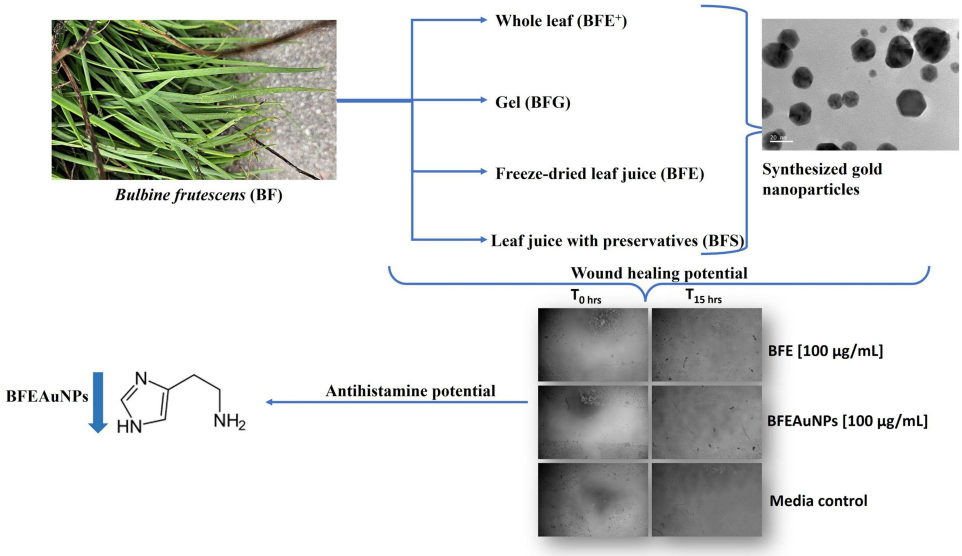

within the skin barrier.[1] The basis of this hypothesis is the loss-of-function mutation within the filaggrin gene, which further impairs the barrier function.[2] The filaggrin gene is located on chromosome 1q21 and translates into a polyprotein known as profilaggrin, which is the main component of keratohyalin granules.[3,4] These profilaggrins are comprised of a calcium-binding N-terminal domain and are dephosphorylated and cleaved into 10–12 filaggrin monomers that contribute to the strength and integrity of the epidermis.[3,5] When these monomers aggregate, the keratin cytoskeleton forms a protein-lipid matrix, which maintains epidermal hydration.[6]

Eczema patients, who have an impaired barrier function, have increased transepidermal water loss and decreased water-binding capacity, which manifests into dry cracked skin.[2,3] Cracked skin causes an increase in histamine production, which leads to an intolerable itching sensation.[7] Increased levels of histamine can, furthermore, affect the expression of genes associated with maintaining the epidermal barrier including filaggrin, keratins and proteases. In response to this, filaggrin levels are reduced and the mRNA expression of some keratins is downregulated, further drying the skin and leading to more severe cracks.[8,9]

Recently, various nanotechnologies have been incorporated into eczema treatments. A review written by Damiani et al (2019) indicated how nanotechnology, when incorporated with current synthetic treatments such as cyclosporine A, corticosteroids and interleukin targeted therapy, enhanced skin penetration, improved drug release and enhanced the drug's activity.[10] However, there is currently no report on the benefit nanotechnology may have on alternative eczema treatments.

Bulbine frutescens (L.) Willd, part of the Asphodelaceae family, is found in southern and eastern Africa and is indigenous to South Africa, where it is mainly located in the Free State, KwaZulu-Natal and in the Cape Province of South Africa.[11,12] *Bulbine frutescens* is used in traditional medicine to treat numerous ailments and conditions. The leaf sap is prepared into a warm poultice for the treatment of wounds, eczema and arthritis.[11,12] An infusion prepared from fresh leaves is used by Rastafarians for coughs and colds.[13] The jelly-like juice within the leaves is used for burns, blisters, cracked lips, acne and mouth ulcers.[13] Other traditional uses of *B. frutescens* include treating diarrhea, ringworms, herpes and insect bites using dried leaf bases.[14,15] *Bulbine frutescens* has not been evaluated for its effect on eczema-associated symptoms; therefore, this study aimed to determine whether extracts prepared from *Bulbine frutescens* alleviated skin damage through wound healing and reduced the production of histamine.

In the cosmetic industry, various nano-delivery systems are used including gold and silver which have been utilized due to their antibacterial and antifungal properties. These delivery systems and their use in the cosmetic industry have been summarized in Table 1.

Table 1 Cosmetic Use of Various Nano-Delivery Systems and Their Benefits[40]

Nano-Delivery Systems	Cosmetic Use	Advantage
Titanium dioxide nanoparticles	Used in any topical treatment that claims to have UV protection including sunscreens, moisturizers and lip balms. Provides more protection against UVB.	Easily absorbed, non-oily and a UV filter
Silver nanoparticles	Wound disinfectant and used as a preservative in toothpaste and shampoo.	Broad antimicrobial activity and can be used as a preservative.
Gold nanoparticles	Wound disinfectant, anti-inflammatory creams, face packs and anti-aging creams	Biocompatible, stable, non-toxicity to cell lines between approximately 1–67 µM/L, antifungal activity, antibacterial properties and displays anti-aging properties by reducing UVA absorption.
Zinc oxide nanoparticles	Mostly used in treatments that reduce the effects of aging caused by UVB radiation and is used in sunscreens and moisturizers	Easily absorbed, non-oily and acts as a UV filter.

Of the nano-delivery systems, gold nanoparticles are mostly used due to their vast benefits in the cosmetic industry. Furthermore, gold nanoparticles have been utilized to repair skin damage and improve skin flexibility making it favorable to use in treating skin inflammation.[17] Akturk et al (2016) reported the potential wound healing activity of gold nanoparticles synthesized using collagen sponges that were cross-linked with glutaraldehyde (CS-AuX). The authors found that CS-AuX under dry testing conditions displayed the highest tensile strength of 1.19 ± 0.40 MPa and a wound closure of 69% compared to the untreated control (45%), which supports the skin repair and flexibility capabilities of gold nanoparticles.[18]

To synthesize gold nanoparticles, various chemical methods can be used; however, these methods are expensive and detrimental to the environment. This has led to the development of "green nanotechnology", which utilizes natural reagents such as plant extracts, bacteria and other organisms as reducing and stabilizing agents. Synthesizing gold nanoparticles using plant extracts became more favorable as the method is cost-effective, simple and environmentally friendly.[19] During this study, green nanotechnology was used to investigate whether gold nanoparticles synthesized using *B. frutescens* would enhance biological activity due to their potential effect on damaged skin cells.

Materials and Methods

Materials, Chemicals and Reagents

The human keratinocytes (HaCaT) were purchased from CELLONEX (Johannesburg, South Africa). The Dulbecco's modified Eagle's Medium (DMEM), Roswell Park Memorial Institute (RPMI-1640) medium, ammonium-chloride-potassium (ACK) lysing buffer, amphotericin B, streptomycin, penicillin, Eutech pH buffer solutions (pH 4, 7 and 10), phosphate-buffered saline (PBS), fetal bovine serum (FBS) and PrestoBlue Cell Viability reagent, were obtained from ThermoFisher Scientific (Johannesburg, South Africa). Cell culture plates and flasks were purchased from LasecSA (Pty) Ltd. (Midrand, South Africa). The histamine (Cat # ab213975) ELISA kit was sourced from BIOCOM Africa (Pty) Ltd. (Lyttleton Manor, South Africa). Phorbol 12-myristate 13-acetate (PMA), histopaque, ethylenediaminetetraacetic acid (EDTA), dimethyl sulfoxide (DMSO), gum arabic, actinomycin D (purity >95%), gold (III) chloride trihydrate ($HAuCl_4.3H_2O$), bovine serum albumin (BSA), sodium chloride (NaCl), gentamicin solution and other chemicals and reagents were obtained from Sigma-Aldrich (Johannesburg, South Africa).

Plant Collection and Extraction

Fresh leaves were collected in March (2016) at the University of Pretoria (UP), the plant material was identified by Ms Magda Nel and a herbarium sample was deposited at the H.G.W.J Schweickerdt Herbarium (PRU number: 122179). The plant species name was validated using http://mpns.kew.org/mpns-portal. Thereafter, a notification (Reference: BABS/

000221N) was submitted and accepted by the Department of Forestry, Fisheries and the Environment (DFFE) in compliance with National Environmental Management: Biodiversity Act, 2004 (Act No. 10 of 2004) (NEMBA).

An ethanolic whole-leaf extract (BFE^+) was prepared by oven drying the leaves and grinding it into a fine powered using an IKA MF10 grinder (MF 10.1 Head 2870900) with a 2 mm sieve. The powdered material was homogenized with absolute ethanol at a 1:5 ratio and agitated on a shaker for 48 hours. Thereafter, the solution was filtered using a Buchner funnel, with the pulp undergoing a second extraction. The remaining solution was concentrated using a Hei-VAP rotary evaporator from Heidolph™ (Schwabach, Germany). Gel extracts were prepared by scraping the gel from the remaining leaves, filtered using a Buchner funnel and freeze-dried into a powder (BFG).

Two leaf juice solutions were prepared by manually harvesting the leaves during the summer season, washed with water and the juice was extracted using a wine press. Thereafter, the juice was pasteurized using heat, filtered using a 0.5-micron filter and separated into two batches. The first juice solution was freeze-dried for three days (BFE), while preservatives consisting of sodium benzoate and potassium sorbate were added to the second leaf juice solution. Thereafter, the pH of the second batch was reduced to between 4 and 5 using 0.1% citric acid (BFS). The four extracts, namely BFE^+, BFE, BFG and BFS were stored at 4°C.

Synthesis of Gold Nanoparticles

Gold nanoparticles were synthesized using the BFE^+, BFE, BFG and BFS extracts. For BFE, BFE^+ and BFG, the extracts were dissolved in 100 mL of distilled water (dH_2O) (stock concentration of 0.2 mg/mL) and were heated to 60°C. Thereafter, the solutions were centrifuged at 1700 rpms for 10 minutes and the supernatant was collected. Thirty milligrams (30 mg) of gum arabic powder were added to 20 mL of BFE and BFE^+, while 60 mg of gum arabic was added to 40 mL of BFG and the solutions were heated to 60°C. Thereafter, 500 µL of 0.01 M gold salt was added per 20 mL of BFE and BFE^+, while 380 µL of 0.1 M gold salt was added per 20 mL of BFG. To synthesize gold nanoparticles from BFS, 8 mL of BFS was added to 12 mg of gum arabic powder. Afterwards, the solution was heated (60–65°C) and 1 mL of 0.01 M gold salt was added. Each of the synthesized nanoparticles was stored at 4°C.

Characterization of Synthesized Gold Nanoparticles

Ultraviolet-Visible (UV-Vis) Spectrometry

To confirm the formation of gold nanoparticles (AuNPs), a full spectral scan was conducted using ultraviolet-visible spectrometry (UV-Vis) to determine if the surface plasmon resonance (SPR) was similar to gold metal (Au). In a 96-well plate, 100 µL of the AuNPs were added and the absorbance was read between 450 and 800 nm at 50 nm increments using a Victor Nivo plate reader (PerkinElmer, Midrand, South Africa).

In vitro Stability

In vitro stability of the AuNP solutions was evaluated in various mediums consisting of buffer solutions and cell culture media, which included 0.5% BSA, 5% NaCl, pH of 4, 7 and 10, phosphate buffer (pH 6.5), DMEM and RPMI-1640 media. The AuNP solutions were added to the abovementioned mediums at a 1:1 ratio to obtain a final volume of 1.5 mL and were incubated at 37°C. To confirm whether the gold nanoparticles were stable, the SPR peaks (λ_{max}) between 450 and 800 nm (increments of 1) were measured using a Victor Nivo plate reader at 0, 2, 24 (Day 1), 48 (Day 2), 72 (Day 3), 96 (Day 4) and 120 hours (Day 5).

High-Resolution Transmission Electron Microscopy (HRTEM)

High-resolution TEM was used to identify the particle size and shape of the AuNPs. Furthermore, the crystallinity was identified through selected area electron diffraction (SAED). Five microlitres (5 µL) of the AuNP solutions were loaded onto a carbon-coated copper TEM grid and allowed to dry. Thereafter, the grids were loaded into a JEOL JEM-ARM200F double Cs-corrected transmission electron microscope equipped with a large solid angle energy-dispersive spectrometer (EDS) (Akishima, Tokyo, Japan) and images were captured.

Dynamic Light Scattering (DLS)

To determine the hydrodynamic size of the AuNPs, 1 mL of the respective AuNP solutions were transferred into a zeta cell and read using a Zetasizer Nano ZS instrument (Malvern Instruments Ltd., Malvern, Worcestershire, UK). Three reads were conducted, and the averages were obtained.

Zeta Potential

The electrostatic charge of the AuNP solutions was evaluated by transferring 1 mL of the respective AuNP solutions into a cuvette, which was read three times using a Zetasizer Nano ZS instrument and the averages of three reads were recorded.

Fourier Transform Infrared Spectrometry (FTIR)

To identify potential phytochemical groups present in the AuNP solutions, FTIR was conducted, using BFE, BFE^+, BFG and BFS as blanks. The percentage transmittance was detected over an infrared range of 550–4000 cm^{-1} using a Perkin Elmer spectrum 100 FTIR spectrometer (Perkin Elmer, Midrand, South Africa).

Quantification of the Total Phenolic Content Present in the Synthesized Nanoparticles

The total phenolic content was quantified using the Folin Ciocalteu method as described by De Canha et al (2021).[20] A standard curve was prepared using the BFE, BFE^+, BFG and BFS extracts. Serial dilutions of the extracts were prepared in dH_2O resulting in a final concentration range of 4000–31.25 µg/mL for BFE and BFE^+, 2000–15.63 µg/mL for BFG and 50–0.39% for BFS. In a 2 mL Eppendorf tube, 125 µL of 7.5% (w/v) sodium bicarbonate solution (Na_2CO_3) and 125 µL 10% (v/v) Folin Ciocalteu reagent (1 in 10 mL dH_2O) was added to 250 µL of each AuNP solutions and each dilution of the extracts. Thereafter, 100 µL of each solution was transferred into a 96-well plate and incubated at 30°C for 30 minutes in the dark. Blanks were prepared in the same manner; however, dH_2O was added in place of 10% Folin Ciocalteu. The absorbance was measured at 765 nm using a Victor Nivo plate reader and the phenolic content of each AuNP solution was determined using the equations generated from its respective extract standard curves (BFE: $y = 9\times10^{-5}x + 0.0092$, $R^2 = 0.9887$, BFE^+: $y = 0.0001x + 0.0031$, $R^2 = 0.9992$, BFG: $y = 0.0002x - 0.0137$, $R^2 = 0.9975$ and BFS: $y = 0.0074x + 0.0024$, $R^2 = 0.9924$). The quantified phenolic content was used as the highest stock concentration in each of the bioassays that followed.

Cell Culture

Human keratinocytes (HaCaT) were used to determine the antiproliferative and wound healing activity of the extracts and AuNP solutions. To maintain the HaCaT cells, DMEM media was supplemented with 10% fetal bovine serum (FBS) and 1% antibiotics consisting of penicillin (100 U/mL) and streptomycin (100 µg/mL) and an antifungal agent, amphotericin B (250 µg/mL). The cells were incubated at 5% CO_2 and 37°C until a confluent monolayer formed and were thereafter sub-cultured using 0.25% trypsin-EDTA.

Antiproliferative Activity Against HaCaT Cells

The method as described by Lall et al (2019) was used to evaluate the antiproliferative activity using the PrestoBlue cell viability reagent.[21] In 96-well microtiter plates, cells were seeded into each well at a concentration of 5×10^4 cells/mL and incubated overnight at 37°C and 5% CO_2. Actinomycin D (stock concentration of 1 mg/mL in dH_2O) was used as a positive toxic inducer. Stock concentrations of the BFE, BFE^+ and BFG were prepared at 20 mg/mL (w/v) in DMSO, while BFS and the respective AuNP solutions were added directly (v/v). The samples were diluted two-fold in a 24-well plate containing media. Once the cells adhered, the extracts, BFS, the respective AuNP solution, 20% DMSO and actinomycin D were added in triplicate, resulting in a final concentration ranging between 400 and 3.125 µg/mL for BFE, BFE^+, their respective AuNPs and BFG, 0.05–3.9×10^4 µg/mL for actinomycin D and 10–0.31% for BFS and BFGAuNPs. Media (100% control), PrestoBlue reagent with no cells (0% control) and a 1% DMSO (vehicle) control were included. After 72 hours, PrestoBlue reagent was added and incubated for a further two hours. Thereafter, the fluorescence was measured at an excitation/emission wavelength of 560/590 nm using a Victor Nivo plate reader. To

calculate the cell viability of each sample, the following equation was used, whereafter the IC_{50} value was calculated using GraphPad Prism 4.

$$\%\text{Viability} = \frac{Fluorescence\ sample - Fluorescence\ 0\%\ control}{(Fluorescence\ vehicle\ control - Fluorescence\ 0\%\ control)} \times 100$$

Wound Healing Assay

The wound-healing assay was conducted using a similar method as described by Liang et al (2007), with slight modifications.[22] Briefly, 500 µL of HaCaT cells at a concentration of 1.5×10^5 cells/mL were seeded into a 48-well plate and incubated overnight at 37°C and 5% CO_2. Once a confluent layer formed, a cross was scratched into the cells using a 1 mL pipette tip and the debris was removed by aspirating the media and replacing it with 500 µL fresh complete media. A stock concentration (20 mg/mL) of BFE, BFE^+ and BFG (in DMSO) was diluted in DMEM media to a final concentration of 1 mg/mL. These stock concentrations, BFS and the respective AuNP solutions were added in duplicate in the 48-well plates containing the cells. The final test concentration for BFE, BFE^+, their respective AuNPs and BFG was 100 and 50 µg/mL, BFS, BFSAuNPs at 2 and 1% and BFGAuNPs at 10 and 5%. A media (untreated) control and a 0.5% DMSO vehicle control were included (in a final volume of 1.5 mL). Thereafter, the plates were incubated for 15 hours. Images at a magnification of 4× were taken before (0 hours) and after (15 hours) the final incubation period and were processed using ImageJ2 (Fiji, https://imagej.net/software/fiji/), to determine the percentage wound closure. Using ImageJ2, the image type was altered to 8-bit and a bandpass filter was applied. Thereafter, the threshold was adjusted (automatic setting) and minimal radium was applied to enhance the scratch outline. Using the wand tool, the borders of the scratch were selected and the analysis measure function was used to obtain the area. To calculate the percentage of wound closure the following equation was used.

$$\%\text{Wound closure} = \left(\frac{Area\ of\ scratch\ at\ 0\ hours\ of\ scratch\ at\ 15\ hours}{Area\ of\ scratch\ at\ 0\ hours}\right) \times 100\%$$

Thereafter, cell viability was measured using a similar method as described in section 2.6, whereby 30 µL of Prestoblue viability reagent was added to 300 µL of media and incubated for two hours. Thereafter, the same equation mentioned in the section titled "Antiproliferative activity against HaCaT cells" was used to calculate the percentage viability.

Granulocyte Isolation

Granulocytes were isolated due to their ability to produce histamine. A volunteer was selected who had eczema and was above the age of 21 with no history of major diseases. Ethics approval was obtained by the ethics committee of the Faculty of Natural and Agricultural Science (EC120411-046, University of Pretoria, South Africa) complying with the Declaration of Helsinki. The ethics committee approved the use of this cell line provided that an informed consent was obtained. Thus, before the study commenced, an informed written consent was obtained whereby the participant acknowledged that data obtained from the collected sample could be used in this study and that their identity would remain confidential.

To isolate the granulocytes, a method described by Oosthuizen et al (2017) was used, with modifications.[23] Briefly, 15 mL of freshly collected blood was diluted with incomplete (no FBS or antimicrobial agents) RPMI-1640 media at a 1:1 ratio, at room temperature. Thereafter, 15 mL of diluted blood was layered on 7.5 mL of histopaque and centrifuged at 1500×g for 30 minutes. After centrifugation, the erythrocyte layer was collected and transferred into a falcon tube. The erythrocytes and granulocytes were lysed with 10% lysis buffer at a ratio of 1:5 (v/v). After 15 minutes, the cells were centrifuged for seven minutes at 540 x *g* at room temperature. The collected pellet was washed with a buffer containing 45 mL PBS, 0.18 g trisodium citrate and 5 mL pasteurized plasma (8:1:1) and resuspended in complete RPMI-1640 media containing 10% heat-inactivated FBS and 1% gentamicin (10 mg/mL).

Quantification of Histamine

To prepare the samples, granulocytes were stimulated with PMA at a final concentration of 1 µg/mL and seeded in a 48-well plate at a concentration of 1.5×10^5 cells/mL. After a 24-hour incubation at 37°C and 5% CO_2, BFE and BFEAuNPs were added, in

duplicate, at a final concentration of 200, 100 and 50 µg/mL and incubated for 30 minutes. Untreated (media with PMA) control and a 0.25% vehicle control were included. Thereafter, 200 µL of cell supernatant was transferred to a 96-well plate and stored at −80°C until used. Cell viability was measured using ImageJ2 at 20× magnification due to the small size of the stimulated granulocytes, which did not convert PrestoBlue. The average size of the granulocytes, after 30 minutes of incubation, was determined using the following protocol. The image type was set to 8-bit and a bandpass filter was applied. The grey morphology of the image was set to a radius of two pixels with a circular structure element. Thereafter, the background, with a rolling ball of more than 12 pixels, was subtracted. The threshold was adjusted to the automatic setting and a watershed binary option was selected to ensure that cells were recognized as separate objects. The image particle size at 120 infinity pixels,[2] with a circularity of 0.0–1, was measured and the average size was recorded. Thereafter, the same equation as section 2.6 was used to calculate percentage viability, to confirm that modulation of histamine was not due to cell death or proliferation with 20% DMSO used as a toxic inducer.

Histamine, from granulocytes cell supernatant, was quantified using a Histamine ELISA kit, following the manufacturer's protocol. Briefly, the standards were prepared by transferring 50 µL of 250 ng/mL histamine standard stock to assay buffer and serially diluted five times resulting in a final concentration range of 25–0.098 ng/mL. A zero standard was included, which included all the reagents and no histamine standard stock. Thereafter, 100 µL of the standard dilutions and the samples (as prepared above) were added to the goat anti-rabbit IgG-coated 96-well microplate in duplicate. A histamine tracer was added to all the wells except the blank, while a histamine antibody was added to the wells excluding the blank and non-specific binding (NSB) wells. The plate was sealed, incubated on a plate shaker (500 rpms) at room temperature (RT) for one hour and washed using a wash solution. After three washes, 200 µL of streptavidin-horseradish peroxide (SA-HRP) conjugate was added to all the wells except the blank, the plate was sealed and incubated for 30 minutes at RT. After three washes, 200 µL of 3.3',5,5'-tetramethyl-benzidine (TMB) substrate was added and incubated for 30 minutes at RT. Thereafter, 50 µL of stop solution was added, the plate was zeroed against the blank and the optical density (OD) at 450 nm was read using a Victor Nivo plate reader. The net OD was determined by subtracting the average OD of the standards and samples from the average NSB OD. The histamine concentration of the samples was determined using the equation generated from the standard curve, which consisted of the average net OD of the standards.

Statistical Analysis

Results were reported as mean ± standard error (or standard deviation) whereby three repeats were conducted. However, two repeats were conducted for the wound healing assay and histamine quantification due to plate layout limitations. To obtain the IC_{50} values, a nonlinear regression analysis of the sigmoidal dose–response curves (4-parameter logistic) using GraphPad Prism 4 was conducted. Statistical analysis was done using a one-way analysis of variance (ANOVA) followed by Dunnett's multiple-comparison tests (GraphPad, version 4), where $p < 0.05$ (*), $p < 0.01$ (**) and $p < 0.001$ (***) were considered statistically significant.

Results

Characterization of Gold Nanoparticles

Gold nanoparticles were synthesized from the BFE, BFE^{+}, BFG and BFS extracts. During the preparation of the gold nanoparticles, the extract solutions immediately converted from a green or brown color (depending on the extract color) to a wine color once mixed with the gold salt. This was confirmed with UV-Vis as each of the AuNP solutions displayed a wavelength between 540 and 550 nm. Furthermore, the total phenolic content of each nanoparticle was determined to be 2171.62 µg/mL (BFEAuNPs), 2005.57 µg/mL (BFE^{+}AuNPs), 99.41 µg/mL (BFGAuNPs) and 49.01% (BFSAuNPs). To determine the phytochemical groups present, FTIR was conducted at a range of 550 to 4000 cm^{-1} (Figures 1–4A, Table 2).

The average diameter and zeta-potential for each synthesized nanoparticle was found to be 128.7 ± 78.51 and −10.5 (BFEAuNPs), 132.0 ± 96.47 and −14.5 (BFE^{+}AuNPs), 51.82 ± 33.76 and −9.27 (BFGAuNPs) and 289.3 ± 88.68 d. nm and −4.02 mV (BFSAuNPs), respectively. High-resolution TEM was used to evaluate the morphology of the synthesized nanoparticles. As displayed in Figures 1–4B, the morphology of the synthesized nanoparticles consisted mostly of round or hexagonal shapes with one or two triangular shapes, while BFSAuNPs contained irregularly shaped nanoparticles.

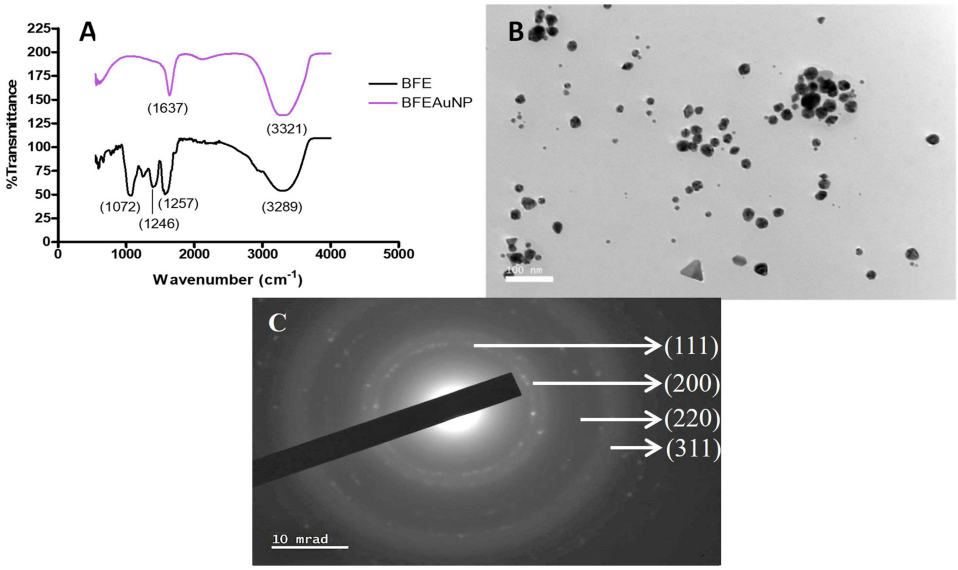

Figure 1 (**A**) Fourier-transform infrared spectrometry (FTIR) of the freeze-dried leaf juice extract (BFE) and synthesized gold nanoparticles (BFEAuNPs), (**B**) high-resolution transmission electron microscopy (HRTEM) and (**C**) selected area diffraction pattern (SAED).

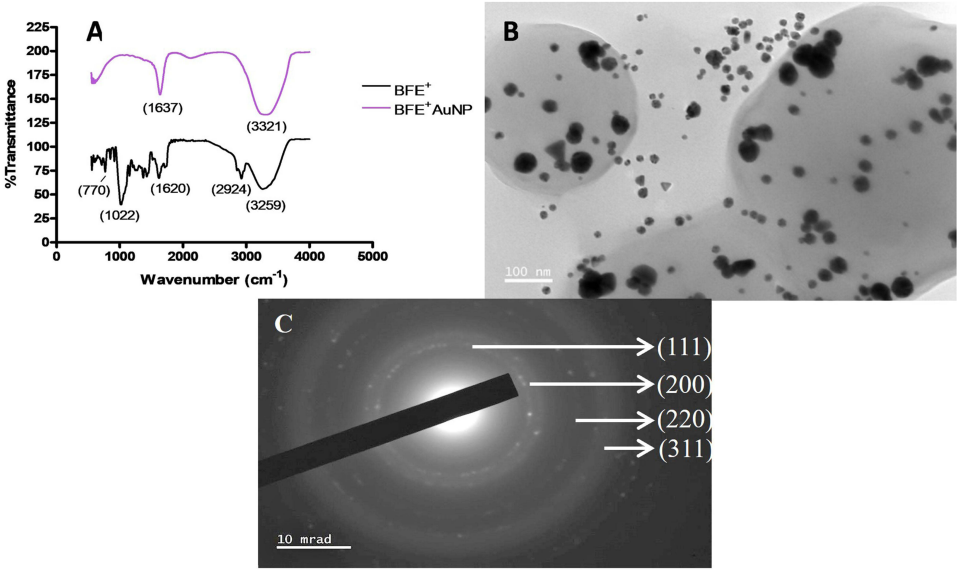

Figure 2 (**A**) Fourier-transform infrared spectrometry (FTIR) of the ethanolic whole leaf extract (BFE+) and synthesized gold nanoparticles (BFE^{+}AuNPs), (**B**) high-resolution transmission electron microscopy (HRTEM) and (**C**) selected area diffraction pattern (SAED).

Furthermore, SAED was used to characterize whether the AuNPs displayed similar lattice planes as gold. If no deviations were observed, this would confirm the stability of the AuNPs. The face-centered lattice planes of each of the synthesized AuNP solutions displayed a diffractive index of (111), (200), (220) and (311) with no deviations (Figures 1–4C).

Lastly, in vitro stability indicated that the AuNP solutions displayed minimal shifts in the surface plasmon resonance peaks (λ_{max}) when added to most of the mediums (Figures 5–8). BFEAuNPs displayed low peaks when added to solutions with a pH level of 7 or containing NaCl (Figure 5). BFE^{+}AuNPs peaks displayed no significant difference when added to the various mediums (Figure 6), while BFGAuNPs and BFSAuNPs showed low peaks when added to BSA (Figures 7 and 8).

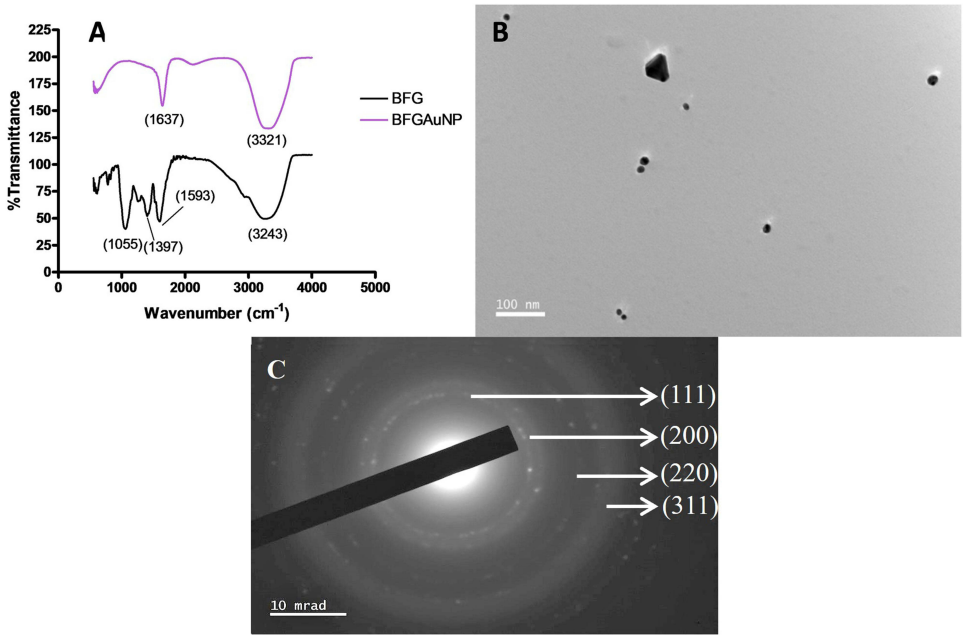

Figure 3 (**A**) Fourier-transform infrared spectrometry (FTIR) of the gel extract (BFG) and synthesized gold nanoparticles (BFGAuNPs), (**B**) high-resolution transmission electron microscopy (HRTEM) and (**C**) selected area diffraction pattern (SAED).

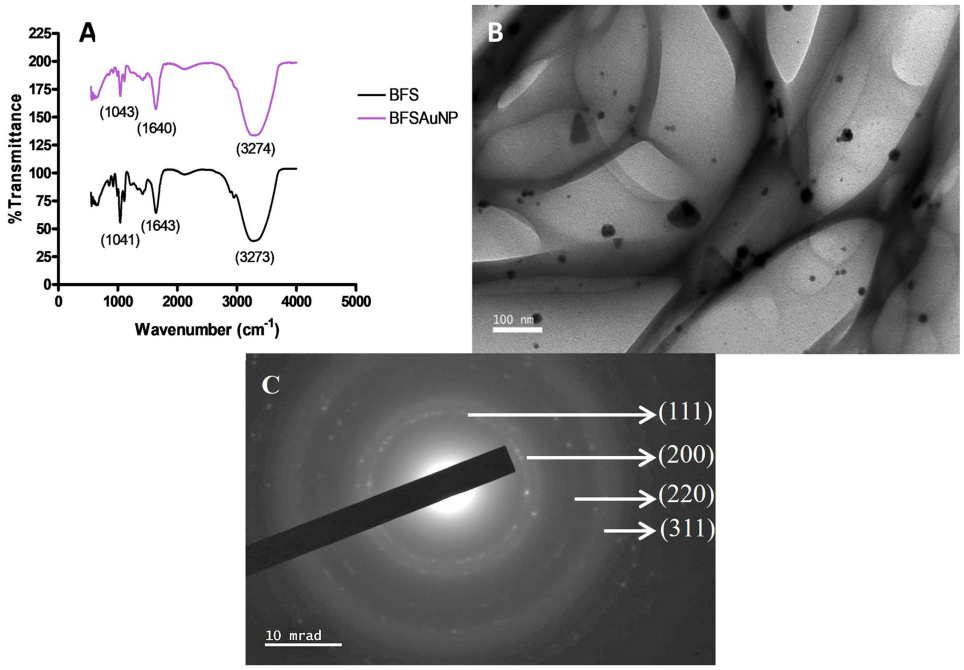

Figure 4 (**A**) Fourier-transform infrared spectrometry (FTIR) of the preserved leaf juice solution (BFS) and synthesized gold nanoparticles (BFSAuNPs), (**B**) high-resolution transmission electron microscopy (HRTEM) and (**C**) selected area diffraction pattern (SAED).

Antiproliferative Activity

BFS and BFSAuNPs displayed antiproliferative activity against HaCaT cells with an IC_{50} of 4.63 ± 0.05 and 3.50 ± 0.40%, while BFE^{+}, BFE, their respective AuNPs and BFG showed $IC_{50} > 400$ µg/mL and BFGAuNPs displayed an $IC_{50} > 10\%$. Samples that displayed significant wound closure were further evaluated for histamine production and were therefore evaluated for anti-proliferative activity against granulocytes. The selected samples, BFE and BFEAuNPs, displayed IC_{50} values >200 µg/mL

Table 2 Potential Functional Groups Were Identified Using Fourier Transform Infrared Spectrometry (FTIR) in Bulbine Frutescens Extracts and Synthesized Gold Nanoparticles (AuNPs)

Functional Group	*Bulbine frutescens* Extract	Transmittance of Extract	Transmittance of AuNP Solutions
Alcohol and phenolic groups (O-H)	BFE [a]	3289	3321
	BFE^{+} [b]	3259	
	BFG [c]	3243	
	BFS [d]	3273	3274
Carboxylic acid	BFE	1246 and 1257	-
Derivatives of carboxylic acid (C=O and O-C bonds)	BFE	-	1637
	BFE+	1620	
	BFG	1593	
	BFS	1643	1640
Phenolic groups (O-H with broad C-O bonds)	BFE	1072	-
	BFE+	1022	-
	BFG	1055	-
	BFS	1041	-

Notes: [a] *Bulbine frutescens* freeze-dried leaf juice extract, [b] *Bulbine frutescens* ethanolic whole leaf extract, [c] *Bulbine frutescens* gel extract, [d] *Bulbine frutescens* preserved leaf juice solution.

Abbreviations: HaCaT, human keratinocytes; IC_{50}, fifty percent inhibitory concentration; DMEM, Dulbecco's Modified Eagle Media; RPMI-1640, Roswell Park Memorial Institute 1640 Medium; ACK, Ammonium Chloride Potassium lysis buffer; PBS, Phosphate-buffered saline; FBS, Fetal bovine serum; EDTA, ethylenediaminetetraacetic acid; PMA, phorbol 12-myristate 13-acetate; DMSO, dimethyl sulfoxide; NaCl, sodium chloride; BSA, bovine serum albumin; AuNPs, gold nanoparticles; UV-Vis, Ultraviolet visible spectrometry; SPR, Surface plasmon resonance; HRTEM, High resolution transmission electron microscopy; DLS, Dynamic Light Scattering; FTIR, Fourier-transform infrared spectrometry; SAED, Selected area electron diffraction; EDS, Energy disperser spectrometer.

against the granulocytes. Moreover, the positive controls (actinomycin D against HaCaT and 20% DMSO against granulocytes) displayed IC_{50} values of 0.01 ± 0.002 µg/mL and 6.06 ± 0.77%, respectively.

Wound Healing Assay

Cell viability of the wound inflicted HaCaT cells was conducted to ensure that test concentrations of the extracts and AuNP solutions did not cause cell death. BFE (93.40 ± 5.15%) and BFG (104.44 ± 11.78%) displayed no significant difference in cell viability when compared to the vehicle control (97.46 ± 3.90%), while BFEAuNPs significantly reduced ($p < 0.01$) cell viability when compared to the untreated control (92.66 ± 3.46%) at a concentration of 400 (74.82 ± 2.98%) and 200 µg/mL (81.08 ± 5.07%). At a concentration of 400 µg/mL, BFE^{+} (49.56 ± 9.10%) significantly reduced ($p < 0.001$) cell viability compared to the vehicle control, while BFE^{+}AuNPs increased ($p < 0.001$) cell viability at 200 (108.80 ± 6.85%), 100 (112.25 ± 0.65%) and 50 µg/mL (109.30 ± 2.69%) compared to the untreated control. Thus, a concentration range of 100 and 50 µg/mL was selected for BFE and BFEAuNPs further evaluation (Figure 9A and B).

BFS significantly ($p < 0.01$) increased cell viability at a concentration of 2% (116.40 ± 9.35%), while BFSAuNPs at 2% (89.65 ± 4.73%) and BFGAuNPs at 10% (84.74 ± 8.28%) displayed no significant difference when compared to the untreated control (92.66 ± 3.46%). Thus, a concentration range of 2 and 1% for BFS and BFSAuNPs and 10 and 5% for BFGAuNPs was selected (Figure 9C).

At a concentration of 100 (31.40 ± 0.88%, $p < 0.01$) and 50 µg/mL (22.22 ± 1.73%, $p < 0.05$), BFE displayed significant wound closure compared to the vehicle control (9.63 ± 0.22%). BFE^{+} (14.34 ± 5.68%) at 100 µg/mL and BFG at 100 (10.47 ± 3.24%) and 50 µg/mL (10.11 ± 3.03%) displayed no effect when compared to the vehicle control.

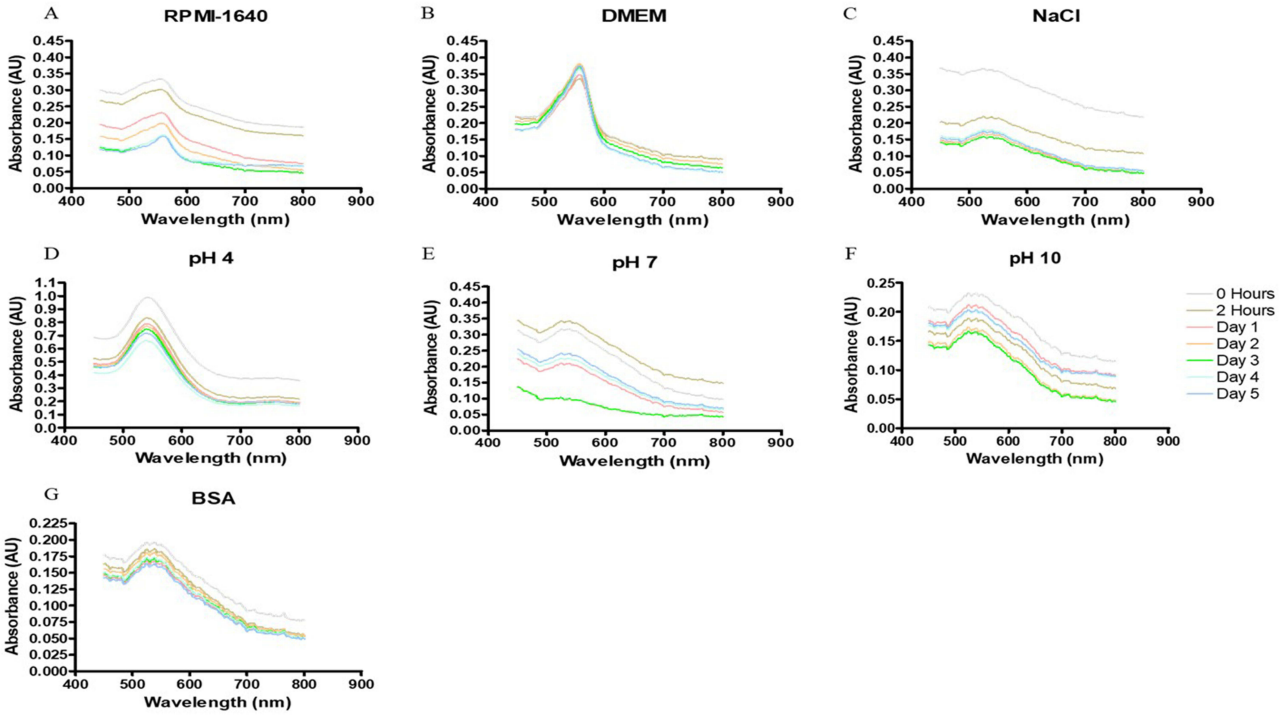

Figure 5 In vitro stability of *Bulbine frutescens* freeze-dried leaf juice synthesized gold nanoparticles (BFEAuNPs) in (**A**) Roswell Park Memorial Institution (RPMI-1640) media, (**B**) Dulbecco's modified Eagle's media (DMEM), (**C**) 5% sodium chloride (NaCl), (**D**) pH of 4, (**E**) 7 and (**F**) 10 and (**G**) 0.5% bovine serum albumin (BSA).

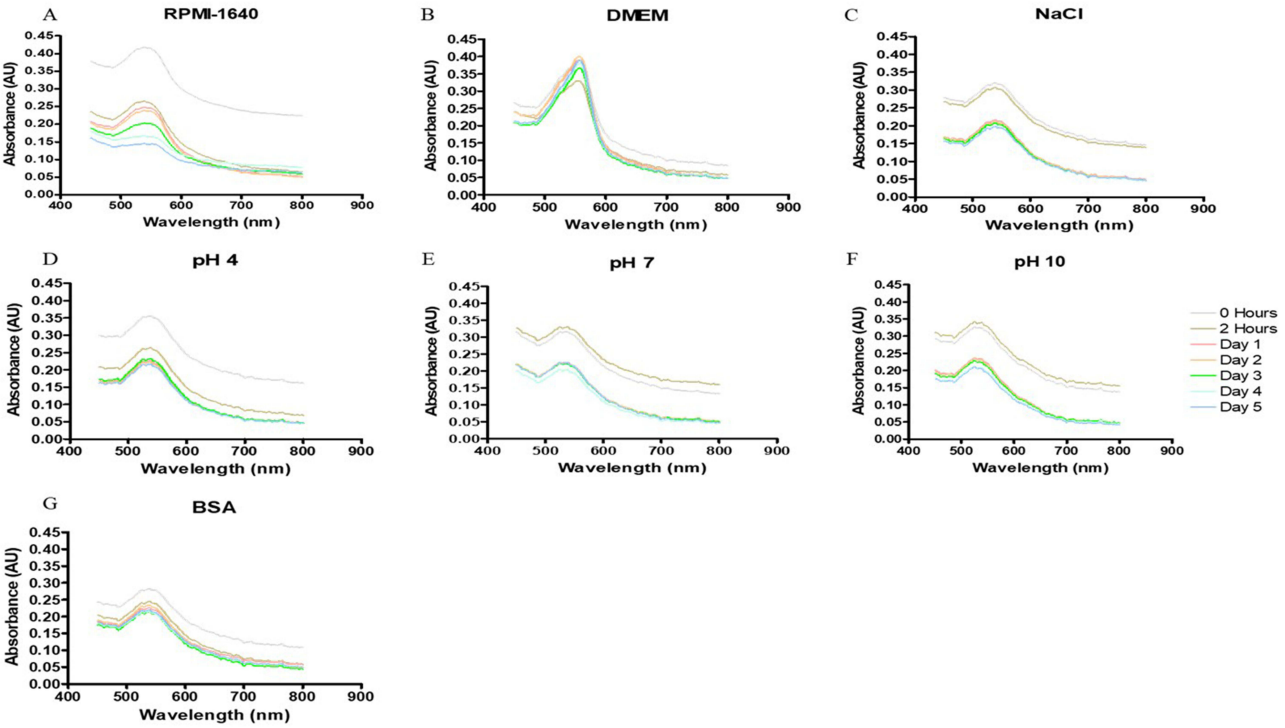

Figure 6 In vitro stability of *Bulbine frutescens* ethanolic whole leaf synthesized gold nanoparticles (BFE^{+}AuNPs) in (**A**) Roswell Park Memorial Institution (RPMI-1640) media, (**B**) Dulbecco's modified Eagle's media (DMEM), (**C**) 5% sodium chloride (NaCl), (**D**) pH of 4, (**E**) 7 and (**F**) 10 and (**G**) 0.5% bovine serum albumin (BSA).

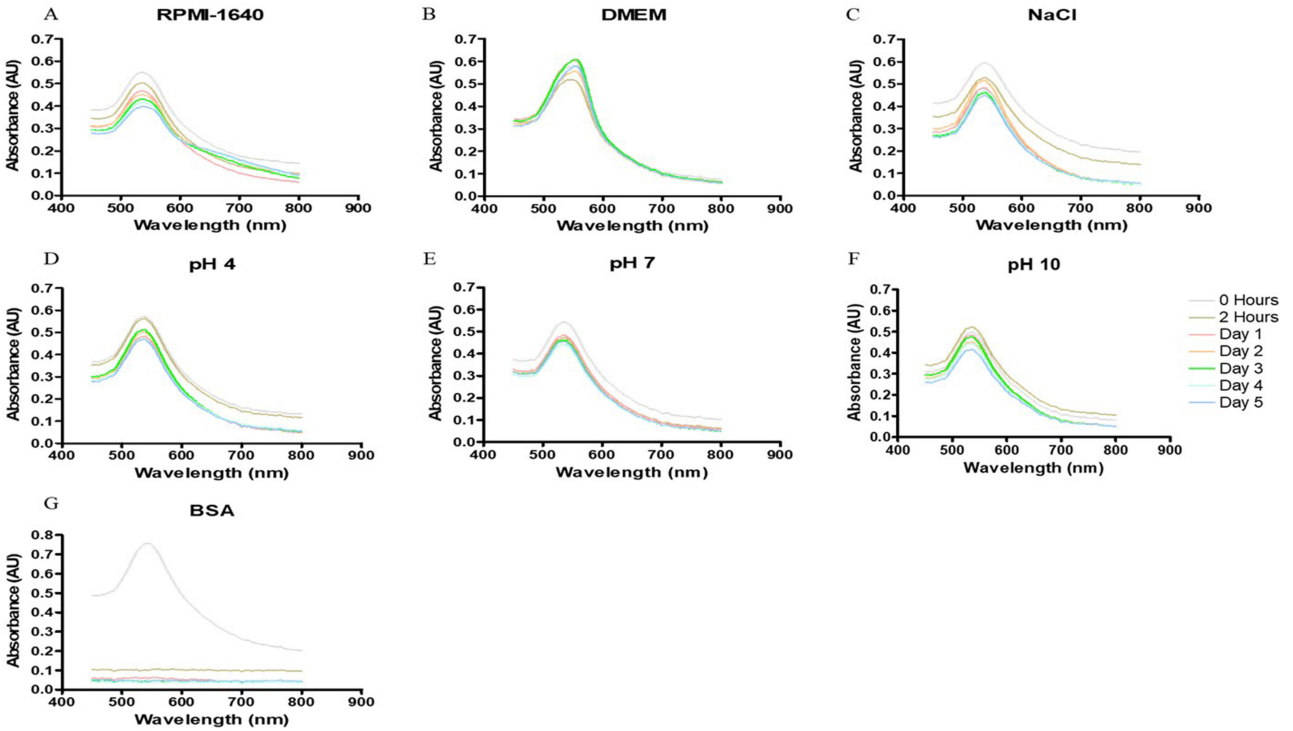

Figure 7 In vitro stability of *Bulbine frutescens* gel synthesized gold nanoparticles (BFGAuNPs) in (**A**) Roswell Park Memorial Institution (RPMI-1640) media, (**B**) Dulbecco's modified Eagle's media (DMEM), (**C**) 5% sodium chloride (NaCl), (**D**) pH of 4, (**E**) 7 and (**F**) 10 and (**G**) 0.5% bovine serum albumin (BSA).

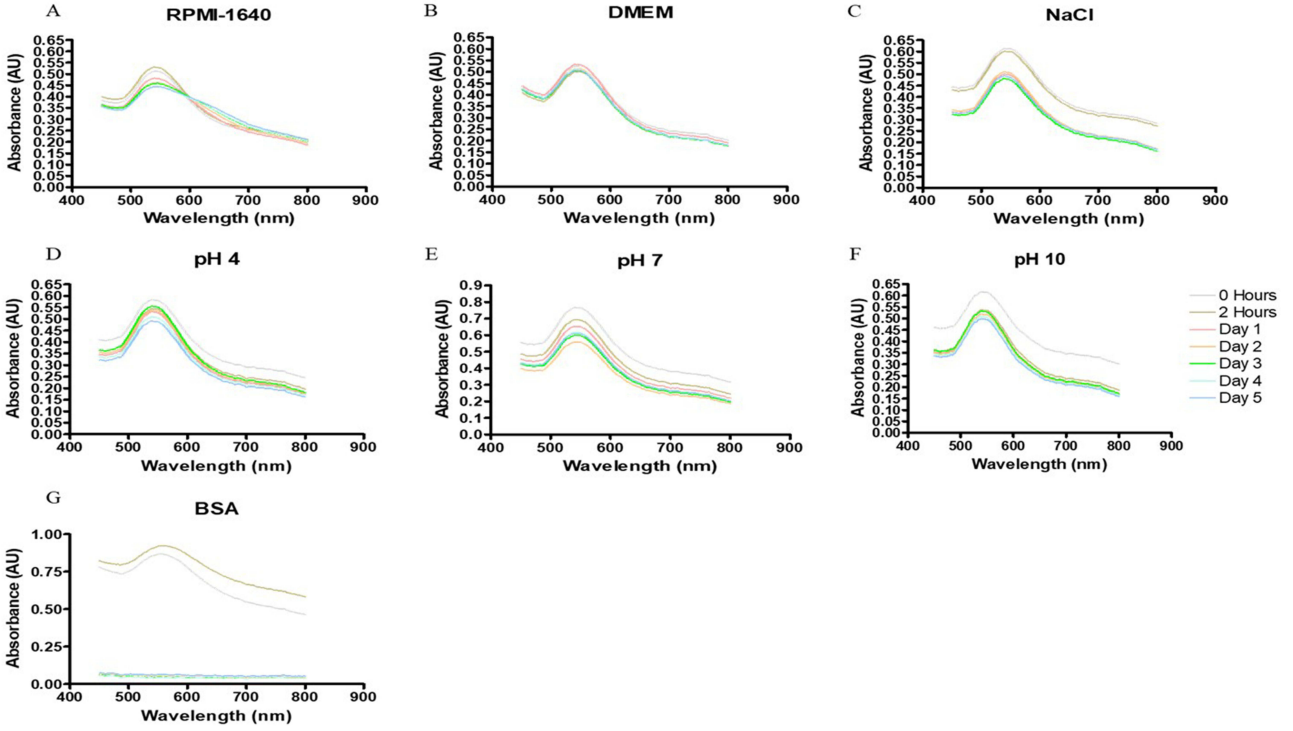

Figure 8 In vitro stability of *Bulbine frutescens* preserved leaf juice synthesized gold nanoparticles (BFSAuNPs) in (**A**) Roswell Park Memorial Institution (RPMI-1640) media, (**B**) Dulbecco's modified Eagle's media (DMEM), (**C**) 5% sodium chloride (NaCl), (**D**) pH of 4, (**E**) 7 and (**F**) 10 and (**G**) 0.5% bovine serum albumin (BSA).

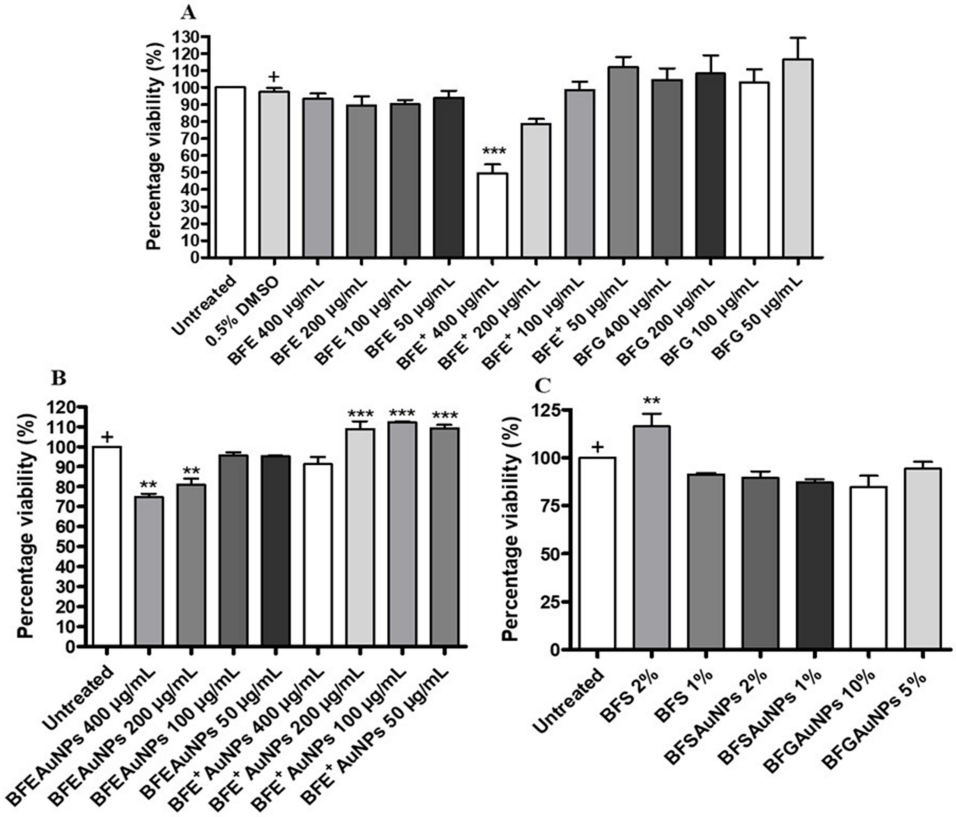

Figure 9 Cell viability of (**A**) BF freeze-dried leaf juice (BFE), ethanolic whole leaf (BFE^+) and gel extract (BFG), (**B**) BF freeze-dried leaf juice synthesized gold nanoparticle (BFEAuNPs) and ethanolic whole leaf synthesized gold nanoparticle (BFE^+AuNPs) solutions at a concentration of 400–50 µg/mL and (**C**) BF preserved leaf juice (BFS), preserved leaf juice synthesized gold nanoparticle (BFSAuNPs) solutions at a concentration of 2 and 1% and gel synthesized gold nanoparticle (BFGAuNPs) solution at 10 and 5% on wound stimulated human keratinocyte (HaCaT) cells. Data represents mean ± SEM (n=2). A significant difference was determined using a one-way ANOVA followed by Dunnett's multiple comparison test, where $p < 0.01$ (**) and $p < 0.001$ (***) indicate significance when compared to the vehicle (0.5% DMSO) and water control (+).

Moreover, BFEAuNPs (20.87 ± 0.69%) at 100 µg/mL significantly enhanced ($p < 0.05$) wound closure, while BFE^+AuNPs (7.91 ± 0.11%) at 100 µg/mL displayed no effect when compared to the untreated control (9.30 ± 0.15%) (Figure 10A and B).

At a concentration of 2 (2.99 ± 2.18%, $p < 0.001$) and 1% (14.71 ± 3.00%, $p < 0.01$) for BFS and 2% for BFSAuNPs (21.54 ± 4.09%, $p < 0.05$), a significant reduction in wound closure was observed compared to the untreated control (50.70 ± 7.78%). BFSAuNPs at 1% (39.63 ± 3.81%) and BFGAuNPs at 10 (33.88 ± 10.79%) and 5% (32.80 ± 4.74%) displayed no significant difference in wound closure compared to the untreated control (Figure 10C).

Quantification of Histamine

The effects of BFE and BFEAuNPs against histamine production were quantified due to the significant wound closure observed. Cell viability of the PMA-stimulated granulocytes was determined to ensure the modulation of histamine was not due to cell death or proliferation. BFE displayed no significant difference in cell viability compared to the 0.25% DMSO (vehicle control), while BFEAuNPs showed no significant difference compared to the untreated (media with PMA) control (Figure 11).

When compared to the untreated control (0.30 ± 0.02 ng/mL), BFEAuNPs significantly inhibited histamine production at a concentration of 100 (0.12 ± 0.04, $p < 0.01$) and 50 µg/mL (0.02 ± 0.008 ng/mL, $p < 0.001$) (Figure 12B), whereas BFE (0.42 ± 0.02 ng/mL) significantly stimulated ($p < 0.01$) histamine production at the highest concentration (200 µg/mL) when compared to the vehicle control (0.15 ± 0.02 ng/mL) (Figure 12A).

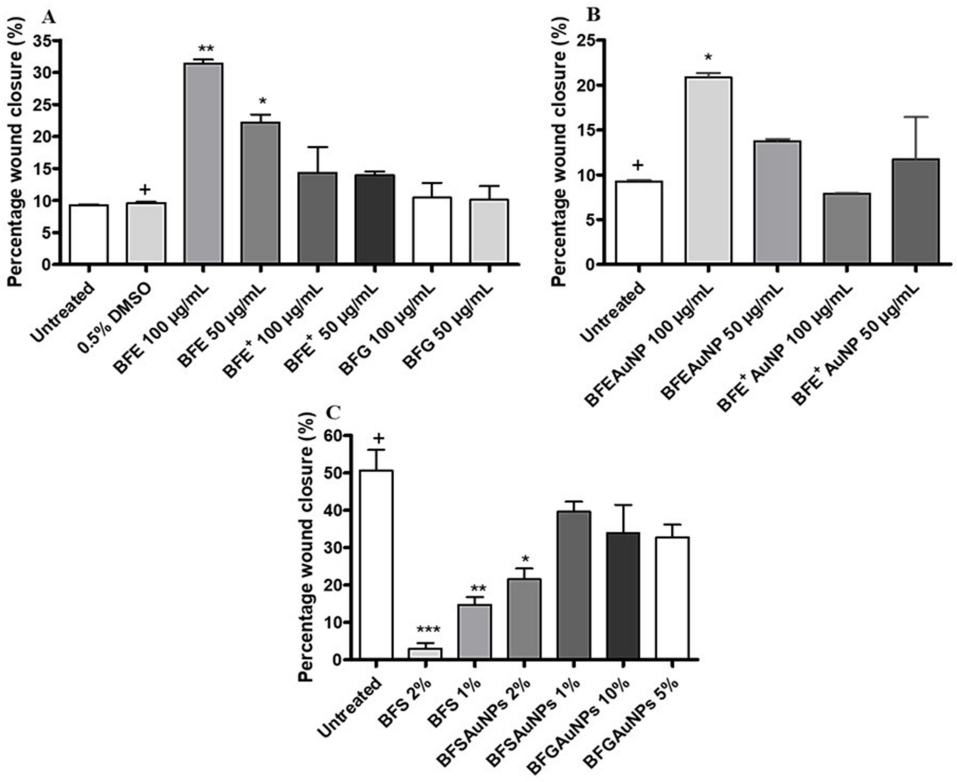

Figure 10 Percentage wound closure of (**A**) BF freeze-dried leaf juice (BFE), ethanolic whole leaf (BFE^+) and gel extract (BFG) at 100 and 50 µg/mL, (**B**) BF freeze-dried leaf juice synthesized gold nanoparticle (BFEAuNPs) and ethanolic whole leaf synthesized gold nanoparticle (BFE^+AuNPs) solutions at 100 and 50 µg/mL and (**C**) BF preserved leaf juice (BFS), preserved leaf juice synthesized gold nanoparticles (BFSAuNPs) at 2 and 1% and gel synthesized gold nanoparticles (BFGAuNPs) at 10 and 5% on human keratinocyte (HaCaT) cells. Data is represented as mean ± SEM (n=2) Significant difference was determined using a one-way ANOVA followed by Dunnett's multiple comparison test, where $p < 0.05$ (*), $p < 0.01$ (**) and $p < 0.001$ (***) indicate significance when compared to the vehicle (0.5% DMSO) control or the untreated control (+).

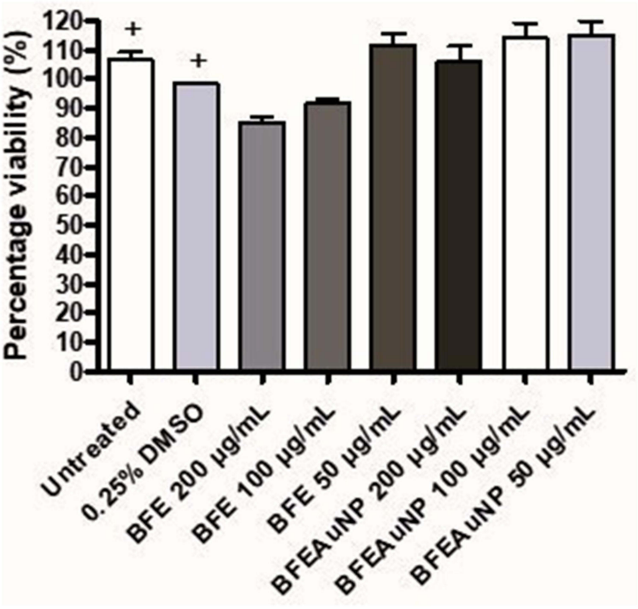

Figure 11 Cell viability of the freeze-dried leaf juice (BFE) extract and synthesized gold nanoparticles using the freeze-dried leaf juice (BFEAuNPs) at a concentration of 200, 100 and 50 µg/mL on phorbol 12-myristate 13-acetate (PMA) stimulated granulocytes. Data represents mean ± SEM (n=2). A significant difference was determined using a one-way ANOVA followed by Dunnett's multiple comparison test when compared to either the untreated (media with PMA) or 0.25% DMSO (vehicle) control (+).

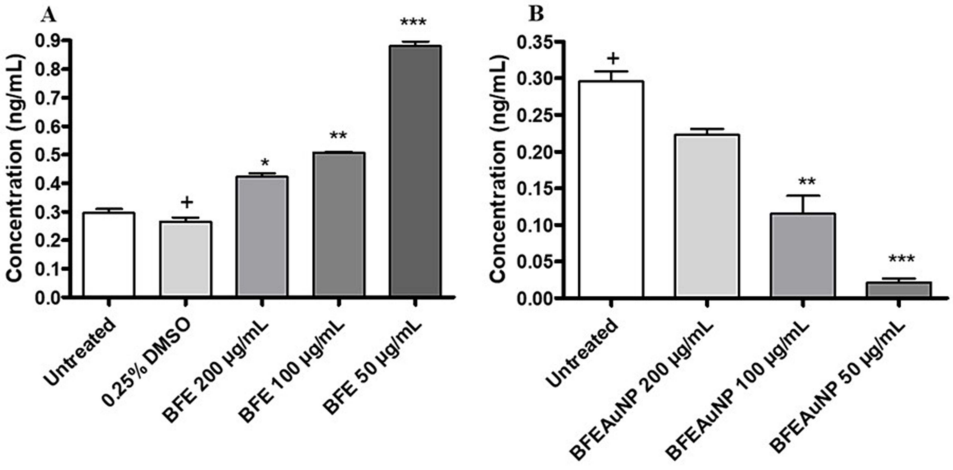

Figure 12 Histamine production of (**A**) BF freeze-dried leaf juice extracts (BFE) and (**B**) BF freeze-dried leaf juice synthesized gold nanoparticles (BFEAuNPs) at a concentration of 200, 100 and 50 µg/mL using phorbol 12-myristate 13-acetate (PMA) stimulated granulocytes. Data represents mean ± SEM (n=2). Significant difference was determined using a one-way ANOVA followed by Dunnett's multiple comparison test, where $p < 0.05$ (*), $p < 0.01$ (**) and $p < 0.001$ (***) indicate significance when compared to either the 0.25% DMSO (vehicle) or untreated (media) control (+).

Discussion

Characterization of the synthesized gold nanoparticles was conducted to identify the potential effect the size, morphology and stability of the AuNPs would have on the biological activity.[20] In a study conducted by Ghuman et al (2016) the phenolic content of a methanol BF leaf extract was evaluated and a weight of 0.29 ± 0.01 mg gallic acid equivalents (GAE) per g dry weight (DW) was found.[24] The total phenolic content of *Helianthus annuus* L. using various solvent systems indicated that the methanol and ethanol extract at 90% and 50% displayed similar results, while the phenolic content of the water extract was significantly lower.[25] This could explain the low phenolic content obtained for BFG as this extract had a high-water content; however, further investigation is required.

The stability of the AuNPs was evaluated in different mediums that mimicked physiological environments. Mediums, where a low SPR peak was observed, could be due to the electrostatic repulsion of the nanoparticle. Gold nanoparticles are considered stable when the zeta potential is above 30 mV or below −30 mV.[26] Furthermore, Salopek et al (1992) indicated that gold nanoparticles begin agglomerating between −10 and −15 mV and display regions of strong agglomeration between 5 and −5 mV.[27] This correlates with the in vitro instability observed for BFEAuNPs (−10.5 mV) when added to NaCl and pH 7 solutions, BFGAuNPs (−9.27 mV) and BFSAuNPs (−4.02 mV) when added to BSA as these samples displayed unstable zeta potential values. Furthermore, agglomeration was observed in the HRTEM image of BFSAuNPs (Figure 4). The agglomeration of BFEAuNPs, BFGAuNPs and BFSAuNPs could have affected the cell viability on HaCaT resulting in the selection of lower concentrations. A review article written by Kus-Liśkiewicz et al (2021) mentioned that aggregated AuNPs displayed toxic effects on dermal fibroblast cells in comparison to non-aggregated particles.[28]

A study conducted by Nguyen et al (2016) indicated that the leaf juice of *Carica papaya* L. significantly reduced cell viability ($p < 0.001$) on HaCaT cells at a concentration of 20 mg/mL.[29] Furthermore, a study conducted by Ying et al (2013) indicated that citric acid at a concentration of 12.5 mM significantly reduced cell viability ($p < 0.001$) on HaCaT cells.[30] Thus, it was suggested that combining citric acid with leaf juice may have resulted in the high antiproliferative activity observed for BFS and BFSAuNPs. However, further studies are required to support this. Similar antiproliferative effects against HaCaT cells for the BFE^{+} and BFG were found in a study conducted by.[31] Jurek et al (2021) indicated that preservatives consisting of sodium benzoate and potassium sorbate at a 1:1 ratio induced cytotoxicity on HaCaT cells.[32] This suggests that the significant reduction in wound closure displayed by BFS and BFSAuNPs could be due to the preservatives used during the preparation of the extract.

Although *B. frutescens* is traditionally used to treat wounds, no studies as of current could be found on its in vitro wound healing effect on HaCaT cells.[33] However, BF leaf extracts have previously displayed significant in vivo wound closure after four days compared to the untreated control when applied topically onto a pig's shaven shin.[34] Furthermore, a compound

isolated from the leaf juice of *B. frutescens*, anthraquinone knipholone, previously displayed high antioxidant activity with an IC_{50} of 22 ± 1.5 µM.[35,36] Excessive reactive oxygen species have previously been reported to reduce wound healing capabilities indicating that anthraquinone knipholone may possess wound healing properties; however, further investigation is required.[37] Moreover, a study conducted by Tambama et al (2014) indicated that a compound previously isolated from *B. frutescens* known as isofuranonaphthoquinone displayed no effect on cell viability at the highest concentration (37.5 µg/mL) compared to the negative control when exposed to Jurkat T cells for 24 hours.[38] Since BFEAuNPs were synthesized using BFE, numerous compounds could have been encapsulated including those that have been mentioned due to their OH groups. However, the identification of compounds in the BFE extract, which may have contributed to the synthesis of BFEAuNPs needs to be investigated to confirm the presence of these compounds.

In a study conducted by Pierson et al (2009), 5-hydroxyindole-2-carboxylic acid amides displayed an inverse agonistic effect on histamine 3-receptor. This receptor when blocked increases the release of histamine.[39] Furthermore, Kubota et al (2009) indicated that a carboxylic acid derivative known as phenothiazineacetic acid binds to histamine 1-receptor, which reduces the production of histamine.[40] This correlates with the results depicted in Figure 12A and B, as BFEAuNPs contain carboxylic acid derivatives while BFE contains carboxylic acid (Table 1).

Conclusion

The potential wound healing and antihistamine properties of *Bulbine frutescens* and whether the synthesis of AuNPs would enhance the biological activity were evaluated. BFE and BFEAuNPs significantly increased wound closure at 100 µg/mL; however, only BFEAuNPs displayed antihistamine activity. Further investigations into the potential in vivo wound healing properties of BFEAuNPs and whether it targets histamine-associated receptors on mast cells as a potential mode of action should be considered. Furthermore, the cellular uptake efficiency of BFEAuNPs into the mast cells should be determined to evaluate the samples effect on the conversion of histidine to histamine by reducing the expression of histidine decarboxylase within the cell.

Acknowledgments

The authors would like to acknowledge Mrs. Bianca D. Payne Department of Plant and Soil Sciences, University of Pretoria) for her guidance and Mrs. Tenille Esmear (Department of Plant and Soil Sciences, University of Pretoria) for assisting with synthesizing the gold nanoparticles. Lastly, the authors would like to thank the Department of Science and Innovation (DSI) for funding contributions.

Funding

The authors report grant from the National Research Foundation (NRF) during the conduct of the study [grant number 98334].

Disclosure

The authors report no conflicts of interest in this work.

References

1. Brandt EB, Sivaprasad U. Th2 Cytokines and Atopic Dermatitis. *J Clin Cell Immunol*. 2011;2(3):1–25. doi:10.4172/2155-9899.1000110
2. Sullivan M, Silverberg NB. Current and emerging concepts in atopic dermatitis pathogenesis. *Clin Dermatol*. 2017;35(4):349–353. doi:10.1016/j.clindermatol.2017.03.006
3. Lee H, Lee S. Epidermal permeability barrier defects and barrier repair therapy in atopic dermatitis. *Allergy Asthma Immunol Res*. 2014;6(4):276–287. doi:10.4168/aair.2014.6.4.276
4. Palmer CNA, Irvine AD, Terron-Kwiatkowski A, et al. Common loss-of-function variants of the epidermal barrier protein filaggrin are a major predisposing factor for atopic dermatitis. *Nature Genet*. 2006;38(4):441–446. doi:doi:10.1038/ng1767
5. Brown SJ, McLean WHI. One remarkable molecule: filaggrin. *J Invest Dermatol*. 2012;132(3):751–762. doi:10.1038/jid.2011.393
6. Voisin T, Chiu IM. Molecular link between itch and atopic dermatitis. *Proc Natl Acad Sci*. 2018;115(51):12851–12853. doi:10.1073/pnas.1818879115
7. Buddenkotte J, Maurer M, Steinhoff M. Histamine and antihistamines in atopic dermatitis. In: *Histamine in Inflammation*. Springer; 2010:73–80.
8. Gschwandtner M, Mildner M, Mlitz V, et al. Histamine suppresses epidermal keratinocyte differentiation and impairs skin barrier function in a human skin model. *Allergy*. 2013;68(1):37–47. doi:10.1111/all.12051

9. Gutowska-Owsiak D, Greenwald L, Watson C, Selvakumar T, Wang X, Ogg G. The histamine-synthesizing enzyme histidine decarboxylase is upregulated by keratinocytes in atopic skin. *Br J Dermatol*. 2014;171(4):771–778. doi:10.1111/bjd.13199
10. Damiani G, Eggenhöffner R, Pigatto PDM, Bragazzi NL. Nanotechnology meets atopic dermatitis: current solutions, challenges and future prospects. Insights and implications from a systematic review of the literature. *Bioact Mater*. 2019;4:380–386. doi:10.1016/j.bioactmat.2019.11.003
11. Abdissa N, Heydenreich M, Midiwo JO, et al. A xanthone and a phenylanthraquinone from the roots of *Bulbine frutescens*, and the revision of six seco-anthraquinones into xanthones. *Phytochem Lett*. 2014;9:67–73. doi:doi:10.1016/j.phytol.2014.04.004
12. Hoffman -D-D Snake Flower – Bulbine frutescens. Available from: https://herbclass.com/bulbine-frutescens/. Accessed 28, April, 2020.
13. Harris S Bulbine frutescens. Available from: http://pza.sanbi.org/bulbine-frutescens. Accessed 28, April, 2020.
14. Pather N, Kramer B. *Bulbine natalensis* and *Bulbine frutescens* promote cutaneous wound healing. *J Ethnopharmacol*. 2012;144(3):523–532. doi:10.1016/j.jep.2012.09.034
15. Coopoosamy R. Traditional information and antibacterial activity of four Bulbine species (Wolf). *Afr J Biotechnol*. 2011;10(2):220–224.
16. Yadwade R, Gharpure S, Ankamwar B. Nanotechnology in cosmetics pros and cons. *Nano Express*. 2021;2(2):022003. doi:10.1088/2632-959X/abf46b
17. Gupta V, Mohapatra S, Mishra H, et al. Nanotechnology in cosmetics and cosmeceuticals—A review of latest advancements. *Gels*. 2022;8(3):173. doi:10.3390/gels8030173
18. Akturk O, Kismet K, Yasti AC, et al. Collagen/gold nanoparticle nanocomposites: a potential skin wound healing biomaterial. *J Biomater Appl*. 2016;31(2):283–301. doi:10.1177/0885328216644536
19. Ikram S. Synthesis of gold nanoparticles using plant extract: an overview. *Nano Res*. 2015;1(1):5.
20. De Canha MN, Thipe VC, Katti KV, et al. The activity of gold nanoparticles synthesized using Helichrysum odoratissimum against Cutibacterium acnes biofilms. *Front Cell Develop Biol*. 2021;2288.
21. Lall N, Blom van Staden A, Rademan S, et al. Antityrosinase and anti-acne potential of plants traditionally used in the Jongilanga community in Mpumalanga. *S Afr J Bot*. 2019;126:241–249. doi:doi:10.1016/j.sajb.2019.07.015
22. Liang -C-C, Park AY, Guan J-L. In vitro scratch assay: a convenient and inexpensive method for analysis of cell migration in vitro. *Nat Protoc*. 2007;2(2):329–333. doi:10.1038/nprot.2007.30
23. Oosthuizen C, Arbach M, Meyer D, Hamilton C, Lall N. Diallyl polysulfides from *Allium sativum* as immunomodulators, hepatoprotectors, and antimycobacterial agents. *Journal of Medicinal Food*. 2017;20(7):685–690. doi:doi:10.1089/jmf.2016.0137
24. Ghuman S, Ncube B, Finnie JF, McGaw LJ, Coopoosamy RM, Van Staden J. Antimicrobial Activity, Phenolic Content, and Cytotoxicity of Medicinal Plant Extracts Used for Treating Dermatological Diseases and Wound Healing in KwaZulu-Natal, South Africa. Original Research. *Front Pharmacol*. 2016;7. doi:10.3389/fphar.2016.00320.
25. Ye F, Liang Q, Li H, Zhao G. Solvent effects on phenolic content, composition, and antioxidant activity of extracts from florets of sunflower (Helianthus annuus L.). *Ind Crops Prod*. 2015;76:574–581. doi:doi:10.1016/j.indcrop.2015.07.063
26. Lata K, Arvind K, Laxmana N, Rajan S. Gold nanoparticles: preparation, characterization and its stability in buffer. *A J Nanotechnol Applica*. 2014;17(1):1–10.
27. Salopek B, Krasic D, Filipovic S. Measurement and application of zeta-potential. *Rudarsko-geolosko-naftni zbornik*. 1992;4(1):147.
28. Kus-Liśkiewicz M, Fickers P, Ben Tahar I. Biocompatibility and Cytotoxicity of Gold Nanoparticles: recent Advances in Methodologies and Regulations. *Int J Mol Sci*. 2021;22(20):10952. doi:10.3390/ijms222010952
29. Nguyen TT, Parat M-O, Shaw PN, Hewavitharana AK, Hodson MP. Traditional aboriginal preparation alters the chemical profile of Carica papaya leaves and impacts on cytotoxicity towards human squamous cell carcinoma. *PLoS One*. 2016;11(2).
30. Ying T-H, Chen C-W, Hsiao Y-P, Hung S-J, Chung J-G, Yang J-H. Citric acid induces cell-cycle arrest and apoptosis of human immortalized keratinocyte cell line (HaCaT) via caspase-and mitochondrial-dependent signaling pathways. *Anticancer Res*. 2013;33(10):4411–4420.
31. Nel M, van Staden AB, Twilley D, et al. Potential of succulents for eczema-associated symptoms. *S Afr J Bot*. 2022;147:1105–1111. doi:10.1016/j.sajb.2022.03.030
32. Jurek I, Szuplewska A, Chudy M, Wojciechowski K. Effect of the oat, horse chestnut, cowherb, soy, quinoa and soapwort extracts on skin-mimicking monolayers and cell lines. *J Surfactants Deterg*. 2022;25(2):185–192. doi:10.1002/jsde.12553
33. Hutchings A. *Zulu Medicinal Plants: An Inventory*. University of Natal press; 1996.
34. Pather N, Viljoen AM, Kramer B. A biochemical comparison of the in vivo effects of Bulbine frutescens and Bulbine natalensis on cutaneous wound healing. *J Ethnopharmacol*. 2011;133(2):364–370. doi:10.1016/j.jep.2010.10.007
35. Habtemariam S. Antioxidant activity of Knipholone anthrone. *Food Chem*. 2007;102(4):1042–1047. doi:10.1016/j.foodchem.2006.06.040
36. Prisa D. Effective Microorganisms Improve Growth and Minerals Content in the Medicinal Plant Bulbine frutescens. *Indian J Nat Sci*. 2022;12(70):37763–37770.
37. Wang G, Yang F, Zhou W, Xiao N, Luo M, Tang Z. The initiation of oxidative stress and therapeutic strategies in wound healing. *Biomed Pharmacother*. 2023;157:114004. doi:doi:10.1016/j.biopha.2022.114004
38. Tambama P, Abegaz B, Mukanganyama S. Antiproliferative activity of the isofuranonaphthoquinone isolated from *Bulbine frutescens* against Jurkat T cells. *Biomed Res Int*. 2014;2014:1–14. doi:doi:10.1155/2014/752941
39. Pierson PD, Fettes A, Freichel C, et al. 5-Hydroxyindole-2-carboxylic Acid Amides: novel Histamine-3 Receptor Inverse Agonists for the Treatment of Obesity. *J Med Chem*. 2009;52(13):3855–3868. doi:10.1021/jm900409x
40. Kubota K, Kurebayashi H, Miyachi H, Tobe M, Onishi M, Isobe Y. Synthesis and structure–activity relationships of phenothiazine carboxylic acids having pyrimidine-dione as novel histamine H1 antagonists. *Bioorg Med Chem Lett*. 2009;19(10):2766–2771. doi:10.1016/j.bmcl.2009.03.124